Contributions of Pulsed Operation Along with Proper Choice of the Substrate for Stabilizing the Catalyst Performance in Electrochemical Reduction of CO$_2$ Toward Ethylene in Gas Diffusion Electrode Based Flow Cell Reactors

Yannick Jännsch,* Martin Hämmerle, Elfriede Simon, Maximilian Fleischer, and Ralf Moos

Electrochemical reduction of CO$_2$ is a promising method to close the carbon cycle and thereby contribute to counteracting climate change. A large share of the research is going into the development of new high-performance catalysts. Often, these catalysts are expensive and difficult to synthesize, especially if considering scaling up to the industrial application. The catalyst is, however, only one factor within the complex system of a CO$_2$-electrolyzer with numerous parameters to explore and optimize. Herein, an optimization process relying on a commercial copper nanopowder as a catalyst is reported. By replacing conductive carbon with polytetrafluoroethylene as the base material of the gas diffusion electrode (GDE) and applying a pulsed potential during electrolysis, the average faradaic efficiency for ethylene could be increased from 38% over 20 h to 50% over 100 h. In addition to the five times increased stability of the process, the ethylene-producing current density rises from 106 to 152 mA cm^{-2}, respectively, while hydrogen evolution was simultaneously reduced. Additionally, further investigations on the interplay of GDE base material, binder, current collector, and catalyst on the electrode performance are presented.

Y. Jännsch, M. Hämmerle, R. Moos
Department for Functional Materials
Center of Energy Technology (ZET)
University of Bayreuth
95440 Bayreuth, Germany
E-mail: functional.materials@uni-bayreuth.de

E. Simon, M. Fleischer
Siemens Energy Global GmbH & Co. KG
81739 München, Germany

The ORCID identification number(s) for the author(s) of this article can be found under https://doi.org/10.1002/ente.202200046.

1. Introduction

In the electrochemical reduction of CO$_2$ (CO$_2$RR), electrical energy is used to convert CO$_2$ into a variety of hydrocarbons and oxygenates.[1] The produced hydrocarbons and oxygenates can be used as basic chemicals and further processed into, e.g., synthetic fuels or polymers.[2] An especially valuable product is ethylene. It has an attractive market value and can easily be chemically processed because of its reactive C–C double bond.[3] Additionally, there are direct usage fields, such as fruit ripening.[4]

Already during early studies of CO$_2$RR, it became apparent that copper plays a crucial role in the electroreduction of CO$_2$, as it is the only metal capable of converting CO$_2$ into multicarbon products.[5,6] However, it comes with two challenges. First, electrolysis at copper produces a variety of hydrocarbons and oxygenates, CO, and H$_2$.[7] Hence, the reduction of CO$_2$ competes with the hydrogen evolution reaction (HER). Therefore, precise electrolysis conditions are required to achieve selective production of ethylene. Second, copper catalysts suffer from deactivation over time.[8–10] Typically, the hydrogen evolution increases at the expense of CO$_2$ reduction.[11] While progress has been made in that respect, the degradation has still not yet been fully overcome and remains one of the great challenges in CO$_2$RR.

One way to improve the stability and selectivity of the CO$_2$RR on copper electrodes is the application of a pulsed potential (pulse method). This method utilizes periodic variations in potential to prolong the activity of the electrode. Each cycle contains two potentials within a step-function. During the lower, more cathodic working potential CO$_2$ is reduced. The more anodic regeneration potential periodically interrupts CO$_2$ reduction to restore the activity of the electrode. The beneficial effects of temporary anodic polarization in this context have already been recognized several years ago.[9,10] However only recently, the pulse method gained increased attention within the

CO_2RR research community.[12–17] Our group previously reported results showing increased stability and selectivity using "pseudo-anodic" pulses.[18,19] Pseudo-anodic means that the applied regeneration potential is still below the open circuit potential (OCP) of the system, however, due to polarization from the previous working potential, a small anodic current can be measured. We could further show that electrodes that have already been deactivated over time during operation at a constant potential, could be reactivated by applying pulsed electrolysis.[19] The reason behind the beneficial effect of the method is still under debate. It was suggested that periodic oxidation and re-reduction of the copper surface could lead to better exploitation of the advantages of oxide-derived copper and a rearrangement of the copper surface.[18,20,21] When applying periodic anodic polarization to lead electrodes, the formation/stabilization of catalytically active $PbCO_3$ was observed during cathodic reduction of CO_2 to formate, also hinting at a necessary, oxidized state of the catalyst in this case.[22]

Other studies show that the beneficial effect appears even if no anodic current flows and the surface structure of the electrode remains unchanged.[23,24] An explanation could be intermittent changes in concentrations of reactants and products close to the electrode surface.[14,23,24] Other mechanisms like the prevention of carbon deposition[21] and a lower amount of hydrogen coverage of the surface[25,26] have been proposed as well.

Another challenge with CO_2RR is the increase in current density, as high current densities are imperative for a future industrial application of the technique.[27] The low solubility of CO_2 in aqueous electrolytes imposes a low limit on the current density if the reaction takes place at a two-phase boundary, for example in an H-cell, as it is often used in laboratories for basic experiments.[28,29] Significant progress has been made in that respect by shifting the reaction to a three-phase-boundary, enabling a gaseous supply of CO_2, while keeping the electrode in contact with the electrolyte. To enable that geometry, a special kind of electrode is required, namely a gas diffusion electrode (GDE) (**Figure 1**a).[30–32] Such an electrode combines several features. A porous gas diffusion layer (GDL) allows for CO_2 and gaseous reaction products to migrate through it. It is often followed by a hydrophobic, microporous layer to hinder the electrolyte from flooding the GDL.[33] The catalyst layer is positioned on top of the microporous layer. In that way, the catalyst is in direct contact with the electrolyte, and the gaseous CO_2 feed at a three-phase boundary.

Often, conductive carbon-based GDLs are used.[34–37] They can act as current collectors and GDL simultaneously, facilitating the electrical contacting of the catalyst layer. Recently, nonconductive polytetrafluoroethylene (PTFE)-based GDLs have risen in popularity.[8,23,38,39] In this case, an additional current collector is required, often realized by a thin layer of copper or graphite.[8,23]

The catalyst layer often contains an additional binder.[40–43] As an adhesive, it binds the catalyst to the electrode. Most commonly, it consists of an ionomer, e.g. Nafion, giving it a second function. The binder gets solvated by the electrolyte, resulting in a high proton conductivity. That way, the catalyst can be (partially) covered in it.[41,43] To form a catalyst layer, an ink consisting of the catalyst, the binder, and a solvent can be drop casted or sprayed onto the GDL. The solvent serves as a medium, in which binder and catalyst can be dispersed and homogenized; it evaporates during the coating process. There is evidence that the choice of solvent has an impact on the coverage of the catalyst by the binder, which in turn influences the product distribution during CO_2RR.[43]
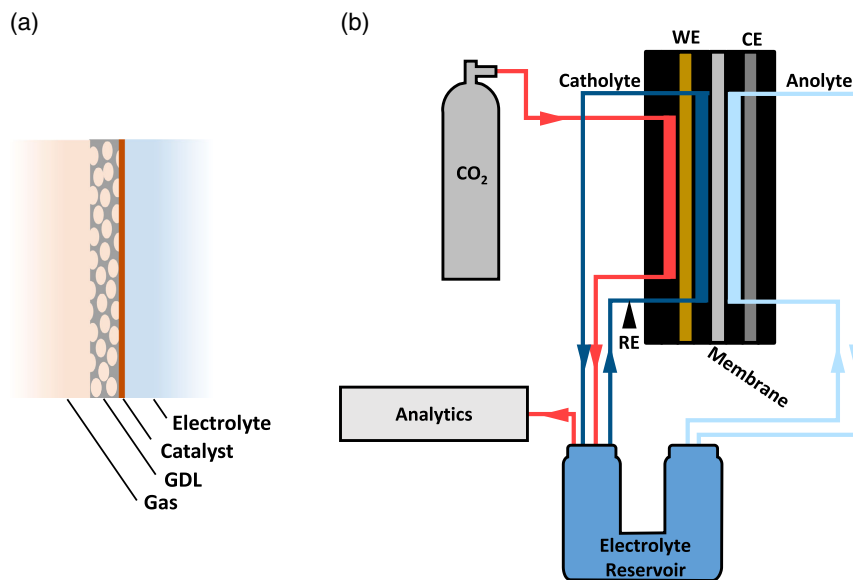

Figure 1. a) Basic principle of a gas diffusion electrode (GDE). A porous gas diffusion layer (GDL) is covered by a catalyst. From the left, a gas can migrate through the GDL to the catalyst layer. From the right, an electrolyte is in contact with the catalyst layer. That way a three-phase boundary among catalyst, electrolyte, and gas phase is realized. b) Scheme of a flow cell setup. WE, CE, and RE denote working electrode, counter electrode, and reference electrode, respectively. An electrolyte is pumped through the cell, separately through the anolyte and catholyte chamber. Gaseous CO_2 is supplied to the cell and the exit gas stream may be redirected toward the on-line analytics. Note that many different configurations for flow cell setups are possible. This particular example resembles the system used in this work.

**ADVANCED
SCIENCE NEWS**
www.advancedsciencenews.com

Energy Technology
Generation, Conversion, Storage, Distribution
www.entechnol.de

To operate a GDE, the cell design has to be redesigned, as an H-cell is not suited for a gaseous CO_2 supply to the surface of the electrode. Instead, flow cells are a common choice.[44] These devices arrange electrodes and optionally membranes together with flow channels for electrolytes and gases.[45] They require peripherals such as pumps and an external electrolyte reservoir. A scheme of a basic flow cell setup is depicted in Figure 1b. Besides the capability of operating GDEs, flow cell setups have the advantage of being scalable, bringing CO_2RR one step closer to industrial application.[28] Most research on the previously mentioned pulse method has been conducted in H-cells, though recently, reports of successfully applying the pulse method to flow cells have also been published.[23,46]

The combination of a multilayered and multifunctional GDE, a flow cell setup, and the option to use dedicated operation techniques such as the pulse method results in a high number of optimizable parameters. In the following, the influence of the different components of the GDE is analyzed and consequently optimized. Finally, the previously discussed pulse method is applied to optimize the system even further. All this is done using the same, commercially available copper powder as a catalyst. The overall aim of this study is to maximize selectivity toward ethylene and the stability of the process while using a cost-effective and highly available catalyst and an application-oriented setup.

2. Experimental Section

2.1. Electrode Preparation

Carbon-based GDEs were prepared using a commercial carbon paper GDL (Freudenberg H23C2). An ink consisting of isopropanol, Nafion (20%, Sigma Aldrich), and copper nanoparticles (40–60 nm, Sigma Aldrich, Lot Nr. MKCL1088) in the weight ratio of 5000:1:10 was prepared and sonicated for 30 min. Then the solution was drop casted onto the GDL. The amount of ink was adjusted to yield a theoretical copper-loading of $1.26\,mg\,cm^{-2}$. The GDL was repeatedly covered with a layer of ink, allowing the solvent to evaporate in-between the repetitions, until the ink was used up. Note that small amounts of catalyst are inevitably lost in the process, lowering the effective copper loading slightly. PTFE-based GDEs were prepared using PTFE-membranes (Sterlitech Aspire Laminated ePTFE membrane QP952). They were coated with a 400 nm layer of copper via physical vapor deposition (PVD) (Univex 450, Leybold). Finally, a catalyst layer was applied on top of the PVD layer via the same drop-casting method as explained previously.

2.2. Electrolysis Experiments

Electrolysis experiments were conducted in a three-compartment flow cell (Micro Flow Cell, Electrocell). The spatial arrangement consisted of a CO_2 compartment, the GDE, a catholyte compartment, a Nafion membrane (N117, Ion Power GmbH), an anolyte compartment, and an iridium mixed metal oxide counter electrode (Electrocell). The electrode area was $10\,cm^2$. An Ag/AgCl (3 M KCl) reference electrode (Metrohm) was installed in the catholyte feed just before the cell. The electrolyte consisted of 340 mL of 1 M $KHCO_3$ and was cycled through the anolyte and catholyte chamber via magnet coupled rotary pumps (March M1) at a flow rate of $10\,L\,h^{-1}$. It has to be emphasized that a common electrolyte in a single reservoir was used. However, the electrolyte was supplied to the cell in two separate lines. A U-shaped electrolyte reservoir allowed for a separate collection of gas bubbles eventually carried within the catholyte and anolyte. $100\,mL\,min^{-1}$ of CO_2 (Rießner Gase, grade 5.5; mass flow controller (Brooks 5850S)) was used as feed gas flow. The gas flow leaving the cell was redirected through the catholyte leg of the reservoir to separate gases and electrolyte. It was then led to a gas chromatograph (GC) (Trace 1310, Thermo Scientific. More information in the Supporting Information.) for on-line quantification. A potentiostat (Autolab PGSTAT302N, Metrohm) with a 10 A booster (Booster10A, Metrohm) was used to control the experiments. More details are shown in the Supporting Information. Figure 1b shows the flow cell setup.

2.3. Figures of Merit

To evaluate the electrolysis experiments, the partial current density for each product was determined according to the following equation

$$j_x = c_x \cdot \frac{QpFz_x}{RTA} \tag{1}$$

where j_x is the current density for product x, c_x is the concentration of the respective product as measured by the GC, Q is the total gas flow, p the ambient pressure, F the Faraday constant, z_x the number of electrons needed to form the respective product, R the gas constant, T the temperature, and A is the electrode area. The current density j_x indicates how much current flows in the formation of each product per square centimeter of the electrode. Based on j_x, the Faradaic efficiency FE_x for each product x was calculated

$$FE_x = \frac{j_x}{|j_{eff}|} \cdot 100\% \tag{2}$$

where j_{eff} stands for the overall current as measured by the potentiostat divided by the electrode area. In theory, the sum of the FEs of all components must be 100%. However, since only gaseous products were analyzed, it is expected to be lower than 100% due to additional liquid products remaining in the liquid electrolyte.

In case of pulsed electrolysis experiments, additional factors have to be considered, with respect to evaluation of the experimental data leading to the correct current density j_x and the correct Faradaic efficiency FE_x. This is described in the Supporting Information.

3. Results and Discussion

3.1. Carbon-Based GDL-Material

As a starting point and benchmark for later experiments, a GDE was prepared via drop-casting an ink containing the copper nanoparticles and Nafion as a binder onto a carbon-based GDL. The GDE was operated in a flow cell setup at $-1.6\,V$ versus Ag/AgCl for 20 h (**Figure 2**). After initially producing high amounts of
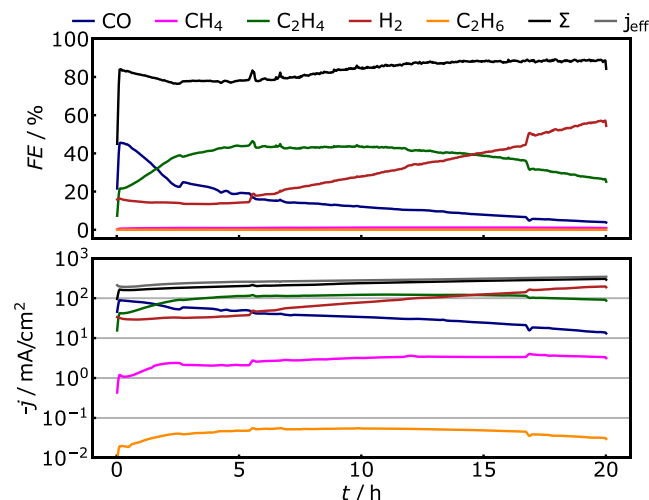
Figure 2. Course of a potentiostatic electrolysis over 20 h using a carbon-based GDE with a copper catalyst layer. The applied potential was −1.6 V versus Ag/AgCl. Decent ethylene selectivity can be observed for multiple hours, however, over time hydrogen evolution starts to dominate while ethylene production decreases.

carbon monoxide, the efficiencies shift and more ethylene is produced at the expense of CO. CO is an intermediate in the formation reaction of ethylene. Thus, it is not surprising that a rising faradaic efficiency for ethylene results in a drop for CO. For the first 5 h, the faradaic efficiency for hydrogen remains at a constant level with a value of less than 20%. After ≈5 h, the FE for hydrogen starts to rise, while the FE for both ethylene and CO decreases. Averaged over 20 h, the ethylene production reaches an FE value of 35% and a current density for ethylene production of 106 mA cm^{-2}. The values for HER are 30% FE and 86 mA cm^{-2}, respectively. The hydrogen production rate surpasses the ethylene FE after 15 h (H$_2$/ethylene crossover point). At the end of the experiment, the HER clearly dominates with 57% FE.

The competition between HER and CO$_2$RR, which eventually leads to increased hydrogen production at the expense of
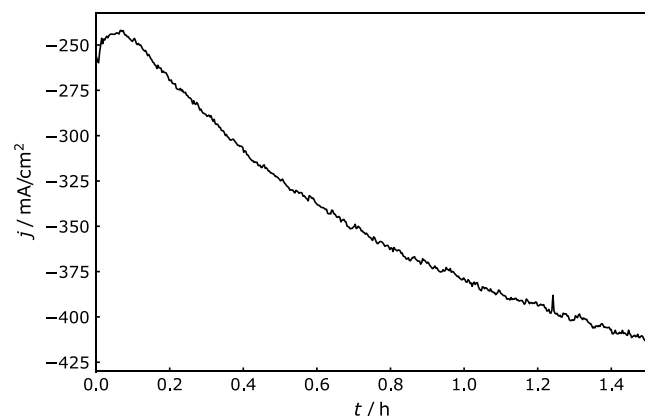

Figure 3. Course of a potentiostatic electrolysis using a carbon-based GDL without copper catalyst at −1.6 V versus Ag/AgCl. H$_2$ was produced exclusively. To increase the signal-to-noise ratio, the current density was averaged over intervals of 10 s before plotting.

hydrocarbons, is often reported for copper catalysts.[11] However, in this case, the hydrogen evolution does not solely rise at the expense of hydrocarbon production, but also independent of it resulting in a rise in total current. To clarify this issue, electrolysis under the same conditions was conducted using a carbon paper GDL without the catalyst ink applied to it. **Figure 3** shows the total current density for electrolysis at −1.6 V versus Ag/AgCl over 90 min. The faradaic efficiency and the partial current densities have been omitted, as the carbon electrode solely produces hydrogen. The graph shows clearly that the absolute value of the current increases by 70% relative to the initial value. The reason for this behavior is reported to be electrowetting of the electrolyte.[47] The carbon GDL possesses a hydrophobic, microporous layer facing the electrolyte. Initially, this prevents the electrolyte from wetting the entire electrode. However, as soon as a current is applied, the effect of electrowetting promotes the intrusion of the electrolyte into the electrode. This results in a rise of the wetted surface area, which explains why the current increases under a constant potential.

Going back to Figure 2, these findings can explain the observed trends. The increase in hydrogen evolution is not only due to the deactivation of the copper catalyst. With increased wetting of the carbon GDL beneath the copper catalyst, the former will contribute to the electrolysis by producing hydrogen. That way, the GDL current collector has turned into an electrochemically active electrode. It can be concluded, that carbon GDLs are disadvantageous for CO$_2$RR, or at least have to be treated with specific care to prevent electrolyte contact.

3.2. PTFE-Based GDL Material

Recently, PTFE-based membranes have become increasingly popular among CO$_2$RR researchers. These membranes consist of a backbone made from polymer fibers. Like the carbon paper GDLs, they have a hydrophobic microporous layer at the top. This layer consists of PTFE. Being gas permeable and hydrophobic, the membranes are in principle suited as GDLs. Advantageously, they are chemically and electrochemically inert. However, this comes with the disadvantage that an additional current collector is needed.

To eliminate any other electrochemically active material from the electrode, it was decided against the use of a graphite layer as a current collector. Instead, a thin copper film was applied to the GDL via PVD. It must be emphasized that this copper film is not supposed to act as a catalyst, but only as a current collector. Nevertheless, it may take part in the electrolysis due to the flooding mechanism previously explained. At that point, a copper current collector is advantageous, as it chemically resembles the catalyst material.

Hence, as a first step, to evaluate the CO$_2$RR performance of the PVD copper layer, electrodes without catalyst applied to it were used for electrolysis. **Figure 4**a shows an electrolysis experiment using a PTFE membrane with a PVD copper layer only. As the scanning electron microscope (SEM) image shows, the PVD copper does not create a continuous film, but instead covers the fibers of the PTFE layer. Also shown is an image from the contact angle (1 M KHCO$_3$) determination. In contrast to the very hydrophobic PTFE (contact angle of 127°, see Supporting
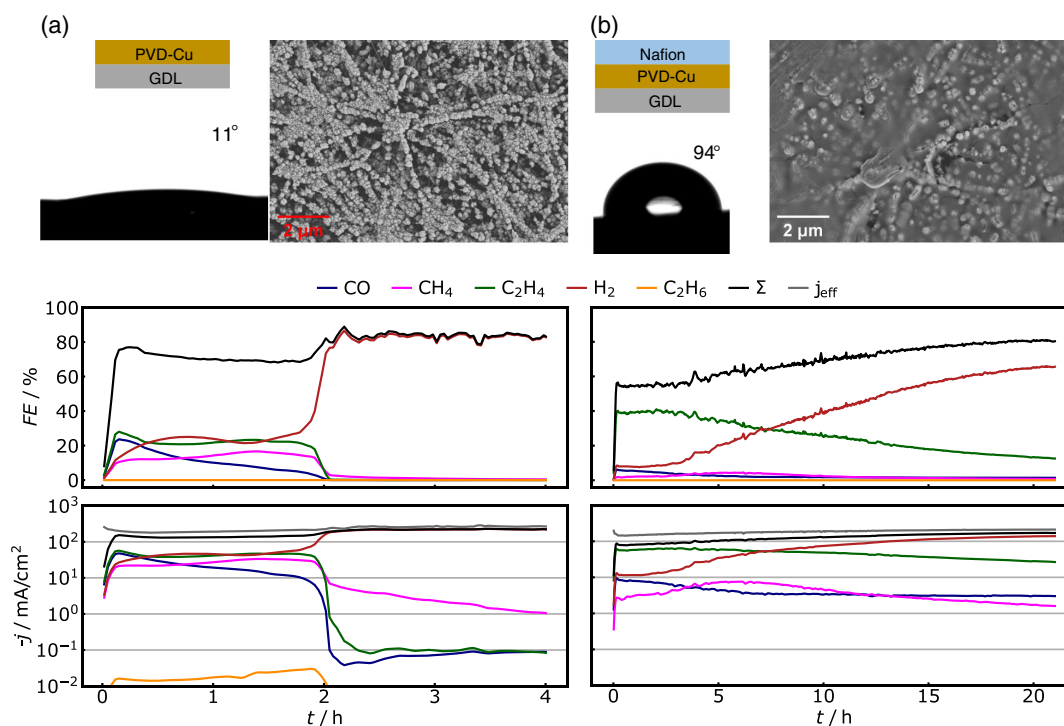
Figure 4. a) Potentiostatic electrolysis at −1.6 V versus Ag/AgCl using a PTFE-GDL with physical vapor deposition (PVD)-Cu but no nanocatalyst/Nafion layer. Severe flooding was observed after 2 h. b) Electrolysis at the same conditions as in (a), but using an electrode with an additional Nafion layer. The electrode could be operated for over 20 h without flooding. Above each plot, a scanning electron microscope (SEM) image of the GDE surface and a schematic layer configuration is displayed as well as an image of an electrolyte droplet on the electrode surface for contact angle determination.

Information), the droplet has an initial contact angle of ≈60° but spreads within seconds to an angle of 11° and lower. This loss in hydrophobicity can be attributed to the copper covering the PTFE fibers. Looking at the electrolysis, a decent selectivity for ethylene above 20% FE can be observed initially, together with an HER rate of comparable size. After two hours, however, a sudden change occurs resulting in exclusive HER and negligible CO_2RR. Severe flooding of the GDE could be observed at this point. The loss in CO_2RR activity can thus be attributed to the inability of CO_2 reaching the reaction site.

Figure 4b shows an experiment, using a similar GDE, but with an additional Nafion layer applied on top of the PVD copper layer via drop-casting. An explicit catalyst is still not applied though. As clearly shown by the SEM image, Nafion fills in the porous structure of the surface of the electrodes. It has to be noted, however, that it is an exception that the underlying PVD copper is visible through the Nafion film as in the SEM image. The majority of the samples showed a plain and featureless Nafion film. To provide contrast and features, the given image was selected. A more typical image can be seen in the Supporting Information. No sudden loss of CO_2RR can be observed over 20 h, as the electrolysis results in Figure 4b show, in contrast to Figure 4a. High selectivity for ethylene is given initially. Over time, the FE of the competing HER rises and dominates after less than 10 h. However, the rise of the total current is much less pronounced in contrast to the carbon paper GDE (Figure 3).

The following conclusions can be drawn. First, the thin PVD copper film has sufficient conductivity to be used as a current collector, but is not well suited as a catalyst on its own. Second, the additional Nafion layer prevents flooding. This may seem counterintuitive at first, as it is solvable, but makes sense at second glance. Figure 4 shows clearly that Nafion closes the porous structure of the GDE, creating a physical barrier and hinders the electrolyte from streaming into the GDE. The contact angle of 94° in Figure 4b at the Nafion-coated surface also indicates better hydrophobicity in comparison to bare copper.

For the following experiments, PTFE-GDLs with a PVD copper layer were coated with a layer consisting of Nafion and the copper nanoparticle catalyst, as used in the preparation of the carbon-based GDEs. The SEM image in **Figure 5** shows a continuous layer of copper particles embedded in Nafion, comparable to the surface structure obtained for the carbon paper GDE (see Supporting Information). The contact angle of 98° resembles the value from Figure 4b, indicating sufficient hydrophobicity. An electrolysis experiment was conducted over 60 h (Figure 5). Selectivity for ethylene increased to a maximum of 52% after 12.3 h. More significantly, the stability increased, shifting the ethylene/H_2 crossover point to 50 h. Over the whole experiment, the values for ethylene averaged at 42.6% FE and 118 mA cm^{-2}, improving on the carbon paper GDE (over 20 h averaged at 35% FE and 106 mA cm^{-2}) despite averaging over threefold the time range. Average HER (23.5% FE and 66 mA cm^{-2}) was lower than on the carbon paper GDE (30% FE and 86 mA cm^{-2}). Again, a deactivation of the catalyst is observed, but the overall current density is stable. It can be summarized that by utilizing PTFE-based GDEs compared to
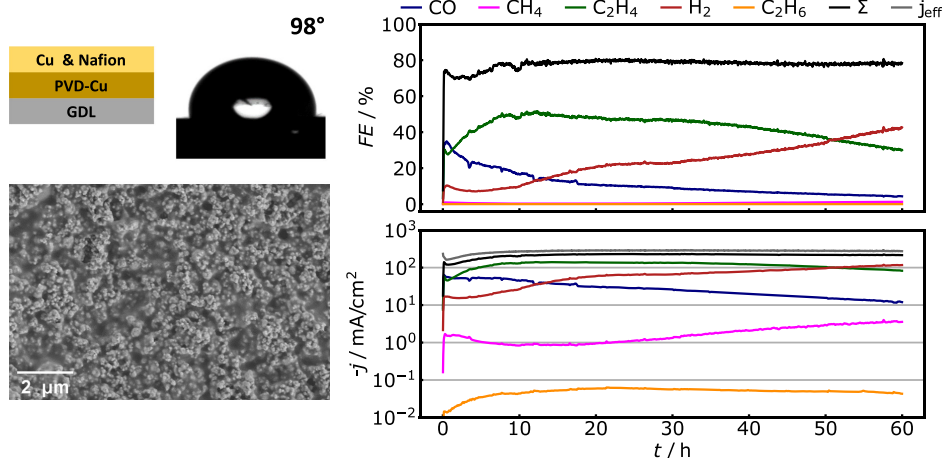
ADVANCED
SCIENCE NEWS
www.advancedsciencenews.com

Energy Technology
Generation, Conversion, Storage, Distribution
www.entechnol.de

Figure 5. Potentiostatic electrolysis (−1.6 V vs Ag/AgCl) over 60 h using a PTFE-based GDE with a PVD-Cu current collector and a drop-casted copper catalyst/Nafion binder layer on top. It shows high ethylene selectivity for more than 50 h. Next to the plot, an SEM-image of the GDE-surface and a schematic layer configuration are displayed as well as an image of an electrolyte droplet on the electrode surface for contact angle determination.

carbon-based GDEs, the CO_2RR performance can be significantly increased. Ethylene selectivity was raised, HER was reduced and the overall current was stabilized.

3.3. Pulsed Electrolysis

To further increase the long-term stability, a pulsed potential was applied during electrolysis. The working potential (−1.6 V vs Ag/AgCl) was identical to the constant potential in the previous experiments. It was interrupted every 2.5 s with a (less cathodic) regeneration pulse of −1.15 V versus Ag/AgCl with a duration of 0.5 s. The course of the potential and the resulting current density over three cycles is depicted in **Figure 6**a. When the potential is increased from −1.6 to −1.15 V, a short anodic spike in the current curve can be observed. This pseudoanodic behavior is due to the polarization of the cathode, making the −1.15 V act anodic for a short time despite being well below the OCP (−120 to −180 mV vs

Ag/AgCl). The anodic current spike varies in height over time, being maximal in the initial phase of the experiment (145 mA cm^{-2} after 12 min). The positive current during the anodic spikes sums up to 0.35% of the entire charge applied during the experiment. Thus, efficiency losses due to the frequent switch in polarization can be neglected. The course of the electrolysis is plotted in Figure 6b. The experiment reveals an overall high selectivity for ethylene, with a maximum of 55.4% FE after 20 h and averaging at a faradaic efficiency of 50.3% and an ethylene-producing current density of 152 mA cm^{-2} over 100 h. A crossover between hydrogen and ethylene production does not occur for the duration of the experiment, however, it is likely to be situated between 120 and 150 h, if extrapolating the data. It can be concluded that the pulse method has a positive impact on both the selectivity toward ethylene and the long-term stability of the electrolysis.

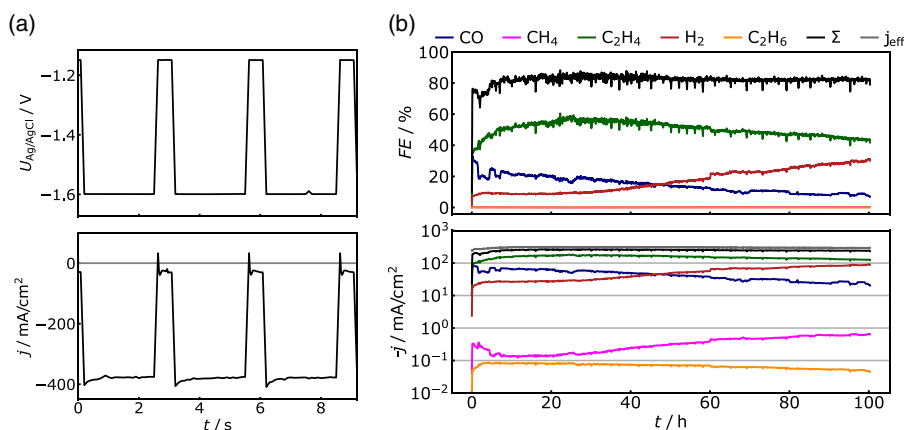The mechanism underlying the positive effects of the pulse method is still under debate. To help toward clarifying the

Figure 6. a) Voltage and current density profiles during pulsed potential electrolysis. It can be observed that short anodic current spikes appear at the start of each regeneration pulse. b) Course of a pulsed potential electrolysis (−1.6 V for 2.5 s as working pulse; −1, 15 V for 0.5 s as regeneration pulse). In comparison to the non-pulsed electrolysis (see Figure 5), the average ethylene selectivity and the long-term stability could be increased further. Over a span of 100 h, ethylene remains the main product, although hydrogen evolution reaction (HER) slightly increases over time.
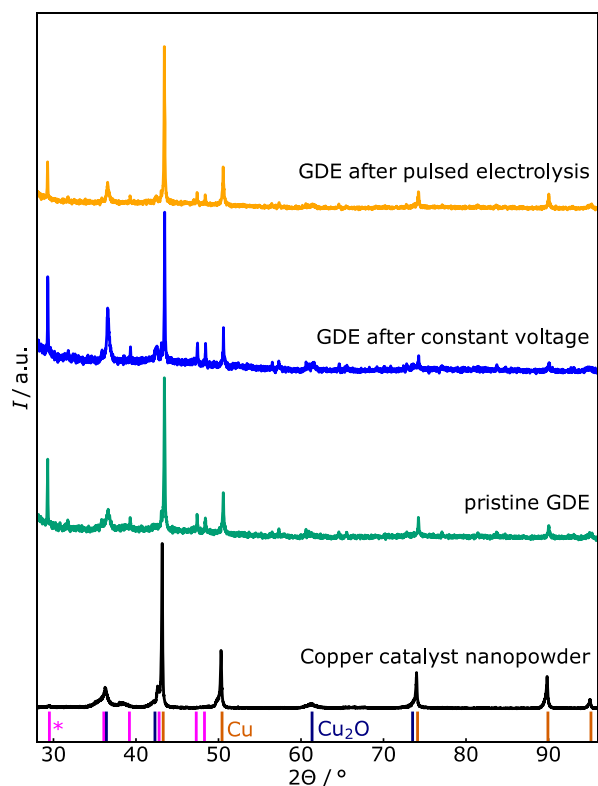
Figure 7. X-ray diffractograms (XRDs) of PTFE-based GDEs show no significant change in catalyst speciation, thus neither the preparation method nor the pulsed electrolysis changes the catalyst itself. (* for fixation knead reflexes, see Supporting Information).

matter, the catalyst was examined before and after electrolysis. **Figure 7** shows four X-ray powder diffractograms (XRD). One of the pristine copper catalyst nanopowder, one of a pristine GDE, and two of used GDEs after constant and after pulsed electrolysis, respectively. A fully indicated plot of the copper nanopowder XRD and further XRDs of GDEs without catalyst as well as of the carbon-based electrodes can be found in the Supporting Information.

Looking at the data of the copper catalyst nanopowder, according to the expectation, mainly copper is identified. A small amount of copper (I) oxide can be observed as well, which agrees with the datasheet (see Supporting Information) of the applied copper particles. Comparing the diffractograms of the copper powder and the pristine GDE, matching reflexes can be observed. A few additional reflexes are apparent. They can be attributed to the fixation knead used during XRD measurements of GDEs (see Supporting Information). There is a difference in the signal-to-noise ratio. This can be explained, as the penetration depth of the XRD exceeds the thickness of the catalyst layer on the GDE. Furthermore, the catalyst on the GDE is embedded in Nafion and thus is present at a reduced density. The reflex position as well as their height ratio is similar for both graphs, indicating that the catalyst did not change chemically during the electrode preparation.

Looking at the two XRDs of the GDEs after electrolysis, the same reflexes as in the pristine case can be observed. After constant electrolysis, the reflexes of the copper(I)oxide appear to have increased in intensity. However, it is questionable, whether the oxidation happened during or after the electrolysis, thus no certain conclusion can be drawn. Thus, the important piece of information that can be extracted from the diffractograms is that
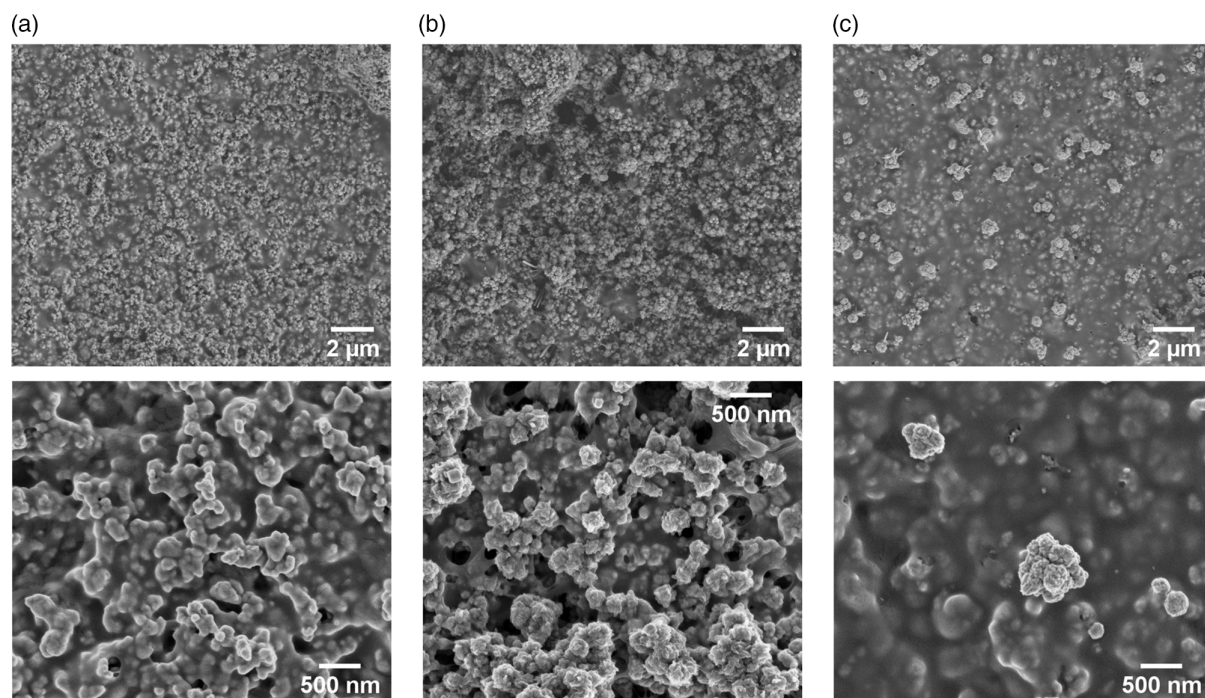

Figure 8. SEM images of the PTFE-based GDEs. a) A pristine GDE, b) a GDE after electrolysis under constant potential, and c) a GDE after pulsed electrolysis are each shown in two different magnifications.

**ADVANCED
SCIENCE NEWS**
www.advancedsciencenews.com

Energy Technology
Generation, Conversion, Storage, Distribution
www.entechnol.de

no significant changes in the bulk chemical composition and oxidation state of the catalyst occur neither during constant nor during pulsed electrolysis. It must be emphasized that for the electrochemical performance of the catalyst/electrode its surface properties are distinctly relevant, however, this is not within the scope of XRD.

Figure 8 shows SEM images of PTFE-based GDEs, pristine and after usage for pulsed and constant electrolysis. In contrast to the XRDs, changes in the visual appearance are apparent. Most strikingly, the amount of visual Nafion changes. Before the electrolysis (Figure 8a), the copper particles are clearly visible but mostly covered in a layer of Nafion. This changes drastically after constant electrolysis (Figure 8b). Despite some Nafion still being visible, exposed copper particles prevail. The latter appear as agglomerates of rough-edged particles. In the picture of lower magnification, an increased surface roughness in comparison to the pristine GDE can be observed. Looking at the images of the GDE after pulsed electrolysis (Figure 8c), yet another surface appearance can be observed. Opposite to the constant electrolysis, the pulsed electrolysis led to a reduction in visible copper particles and a surface dominated by Nafion. The few visible agglomerates of copper particles have a similar shape and appearance in comparison to Figure 8b.

In section 3.2, the beneficial effect of a Nafion layer has been established. Thus, it can be assumed that the higher presence of the binder at the surface during pulsed potential electrolysis is a major factor in prolonging ethylene selectivity and long-term stability. While differences in surface restructuring were observed, further investigations are necessary to reveal the mechanism behind it. In situ methods could prove especially useful in this respect. However, as these require a fundamentally different electrolysis setup, they exceed the scope of this study. It can be summarized that pulsed electrolysis improves long-term stability and selectivity for ethylene production, as was clearly shown in this study. It also does have a significant effect on the surface structure of the electrode (Figure 8), but does not change the bulk chemical state of the copper catalyst (Figure 7).

4. Conclusion

In this study, the influence of the GDL base material, binder (Nafion), and potential control (constant vs pulsed potential) on the selectivity and long-term stability of ethylene production during CO_2RR were investigated and optimized. A commercial copper nanopowder served as a catalyst. By eliminating carbon as an electrochemically active material from the GDE setup, the increase of HER over time could be significantly reduced. Using a PTFE membrane as the GDL, a PVD copper layer as the current collector, and Nafion as the binder, ethylene selective electrolysis could be conducted for over 60 h. The functionalities of all named components were investigated, showing that the PVD copper itself shows some ethylene selectivity, however, significant improvements were achieved when additionally using copper nanopowder as a catalyst. It was also shown that the binder on the GDE acts as a barrier, preventing flooding by the electrolyte. Finally, a pulsed potential method was applied during electrolysis, boosting stability and selectivity for ethylene

production even further, achieving an average faradaic efficiency of 50.3% and an ethylene-producing current density of 152 mA cm^{-2} over 100 h. The mechanism underlying the pulse method is still under debate. The results presented here show that the surface appearance changes drastically when applying pulsed potentials, however, the bulk chemical state of the catalyst remains unchanged.

The results presented in this study originate from a performance-oriented optimization process. New interesting questions concerning the underlying mechanisms arose. They were only briefly addressed via XRD and SEM analysis, as deeper analysis would have gone beyond the scope of this publication. A more detailed and fundamental analysis of the underlying mechanisms is necessary and will be subject to future work. Especially the relation among the pulsed operation, the Nafion coverage, and the local pH at the catalyst surface would be of great interest.

All in all, it can be deduced that the catalyst is only one factor in a complex system, and significant increases in selectivity and long-term stability can also be achieved by tailoring the system around the catalyst instead of solely focusing on the catalyst design. Finding a way to effectively apply cost-effective and highly available catalysts is a promising route to feasible and scalable CO_2RR. Numerous further factors exist, which could not be covered in this study, for example, temperature, pressures, flow rates, electrolyte type and concentration, catalyst loading, or the solvent selection for the ink. These factors and the understanding of their interplay promise further potential for optimization in the future.

Supporting Information

Acknowledgements

Conflict of Interest

The authors declare no conflict of interest.

Data Availability Statement

The data that support the findings of this study are available from the corresponding author upon reasonable request.

Keywords

[1] S. Nitopi, E. Bertheussen, S. B. Scott, X. Liu, A. K. Engstfeld, S. Horch, B. Seger, I. E. L. Stephens, K. Chan, C. Hahn, J. K. Nørskov, T. F. Jaramillo, I. Chorkendorff, *Chem. Rev.* **2019**, *119*, 7610.

[2] R. G. Grim, Z. Huang, M. T. Guarnieri, J. R. Ferrell, L. Tao, J. A. Schaidle, *Energy Environ. Sci.* **2020**, *13*, 472.

[3] J. Sisler, S. Khan, A. H. Ip, M. W. Schreiber, S. A. Jaffer, E. R. Bobicki, C.-T. Dinh, E. H. Sargent, *ACS Energy Lett.* **2021**, 997.

[4] C. S. Barry, J. J. Giovannoni, *J. Plant Growth Regul.* **2007**, *26*, 143.

[5] Y. Hori, S. Suzuki, *J. Res. Inst. Catal. Hokkaido Univ.* **1982**, *30*, 81.

[6] Y. Hori, A. Murata, R. Takahashi, *J. Chem. Soc., Faraday Trans.* **1989**, *1* 2309.

[7] K. P. Kuhl, E. R. Cave, D. N. Abram, T. F. Jaramillo, *Energy Environ. Sci.* **2012**, *5*, 7050.

[8] C.-T. Dinh, T. Burdyny, M. G. Kibria, A. Seifitokaldani, C. M. Gabardo, F. P. García de Arquer, A. Kiani, J. P. Edwards, P. de Luna, O. S. Bushuyev, C. Zou, R. Quintero-Bermudez, Y. Pang, D. Sinton, E. H. Sargent, *Science* **2018**, *360*, 783.

[9] Y. Hori, H. Konishi, T. Futamura, A. Murata, O. Koga, H. Sakurai, K. Oguma, *Electrochim. Acta* **2005**, *50*, 5354.

[10] R. Shiratsuchi, Y. Aikoh, G. Nogami, *J. Electrochem. Soc.* **1993**, *140*, 3479.

[11] Z. Weng, X. Zhang, Y. Wu, S. Huo, J. Jiang, W. Liu, G. He, Y. Liang, H. Wang, *Angew. Chem.* **2017**, *129*, 13315.

[12] R. Casebolt, K. Levine, J. Suntivich, T. Hanrath, *Joule* **2021**, *8*, 1987.

[13] C. S. Le Duff, M. J. Lawrence, P. Rodriguez, *Angew. Chem.* **2017**, *129*, 13099.

[14] R. Casebolt, K. Kimura, K. Levine, J. A. Cimada DaSilva, J. Kim, T. Dunbar, J. Suntivich, T. Hanrath, *ChemElectroChem* **2020**, *4*, 681.

[15] K. W. Kimura, K. E. Fritz, J. Kim, J. Suntivich, H. D. Abruña, T. Hanrath, *ChemSusChem* **2018**, *11*, 1781.

[16] K. W. Kimura, R. Casebolt, J. Cimada daSilva, E. Kauffman, J. Kim, T. A. Dunbar, C. J. Pollock, J. Suntivich, T. Hanrath, K. W. Kimura, J. Cimada daSilva, T. A. Dunbar, J. Cimada daSilva, *ACS Catal.* **2020**, *10*, 8632.

[17] T. Liu, J. Wang, X. Yang, M. Gong, *J. Energy Chem.* **2020**, *59*, 69.

[18] A. Engelbrecht, C. Uhlig, O. Stark, M. Hämmerle, G. Schmid, E. Magori, K. Wiesner-Fleischer, M. Fleischer, R. Moos, *J. Electrochem. Soc.* **2018**, *165*, J3059.

[19] Y. Jännsch, J. J. Leung, M. Hämmerle, E. Magori, K. Wiesner-Fleischer, E. Simon, M. Fleischer, R. Moos, *Electrochem. Commun.* **2020**, *121*, 106861.

[20] R. M. Arán-Ais, F. Scholten, S. Kunze, R. Rizo, B. Roldan Cuenya, *Nat Energy* **2020**, *5*, 317.

[21] J. Lee, Y. Tak, *Electrochim. Acta* **2001**, *46*, 3015.

[22] L. de Sousa, C. Harmoko, N. Benes, G. Mul, *ACS EST Eng.* **2021**, *1*, 1649.

[23] Y. Xu, J. P. Edwards, S. Liu, R. K. Miao, J. E. Huang, C. M. Gabardo, C. P. O'Brien, J. Li, E. H. Sargent, D. Sinton, *ACS Energy Lett.* **2021**, 809.

[24] C. Kim, L.-C. Weng, A. T. Bell, *ACS Catal.* **2020**, 12403.

[25] S. Ishimaru, R. Shiratsuchi, G. Nogami, *J. Electrochem. Soc.* **2000**, *147*, 1864.

[26] Z. Tang, E. Nishiwaki, K. E. Fritz, T. Hanrath, J. Suntivich, *ACS Appl. Mater. Interfaces* **2021**, *12*, 14050.

[27] S. Jiao, X. Fu, L. Zhang, L. Zhang, S. Ruan, Y.-J. Zeng, H. Huang, *Nano Today* **2021**, *36*, 101028.

[28] D. M. Weekes, D. A. Salvatore, A. Reyes, A. Huang, C. P. Berlinguette, *Acc. Chem. Res.* **2018**, *51*, 910.

[29] A. Engelbrecht, M. Hämmerle, R. Moos, M. Fleischer, G. Schmid, *Electrochim. Acta* **2017**, *224*, 642.

[30] K. Liu, W. A. Smith, T. Burdyny, *ACS Energy Lett.* **2019**, *4*, 639.

[31] T. Burdyny, W. A. Smith, *Energy Environ. Sci.* **2019**, *12*, 1442.

[32] S. Malkhandi, B. S. Yeo, *Curr. Opin. Chem. Eng.* **2019**, *26*, 112.

[33] B. Kim, F. Hillman, M. Ariyoshi, S. Fujikawa, P. J. Kenis, *J. Power Sources* **2016**, *312*, 192.

[34] N. S. Romero Cuellar, K. Wiesner-Fleischer, M. Fleischer, A. Rucki, O. Hinrichsen, *Electrochim. Acta* **2019**, *307*, 164.

[35] M. Wu, C. Zhu, K. Wang, G. Li, X. Dong, Y. Song, J. Xue, W. Chen, W. Wei, Y. Sun, *ACS Appl. Mater. Interfaces* **2020**, *10*, 11562.

[36] M. Fan, Z. Bai, Q. Zhang, C. Ma, X.-D. Zhou, J. Qiao, *RSC Adv.* **2014**, *4*, 44583.

[37] Z. Chen, T. Wang, B. Liu, D. Cheng, C. Hu, G. Zhang, W. Zhu, H. Wang, Z.-J. Zhao, J. Gong, *J. Am. Chem. Soc.* **2020**, *15*, 6878.

[38] F. P. García de Arquer, C.-T. Dinh, A. Ozden, J. Wicks, C. McCallum, A. R. Kirmani, D.-H. Nam, C. Gabardo, A. Seifitokaldani, X. Wang, Y. C. Li, F. Li, J. Edwards, L. J. Richter, S. J. Thorpe, D. Sinton, E. H. Sargent, *Science* **2020**, *367*, 661.

[39] K. Junge Puring, D. Siegmund, J. Timm, F. Möllenbruck, S. Schemme, R. Marschall, U.-P. Apfel, *Adv. Sustainable Syst.* **2020**, *52*, 2000088.

[40] U. O. Nwabara, A. D. Hernandez, D. A. Henckel, X. Chen, E. R. Cofell, M. P. de-Heer, S. Verma, A. A. Gewirth, P. J. A. Kenis, *ACS Appl. Energy Mater.* **2021**, *5*, 5175.

[41] E. Antolini, L. Giorgi, A. Pozio, E. Passalacqua, *J. Power Sources* **1999**, *77*, 136.

[42] J. H. Lee, S. Kattel, Z. Xie, B. M. Tackett, J. Wang, C.-J. Liu, J. G. Chen, *Adv. Funct. Mater.* **2018**, *28*, 1804762.

[43] M. J. Blom, V. Smulders, W. P. van Swaaij, S. R. Kersten, G. Mul, *Appl. Catal., B* **2020**, *268*, 118420.

[44] M. Bevilacqua, J. Filippi, H. A. Miller, F. Vizza, *Energy Technol.* **2015**, *3*, 197.

[45] S. Liang, N. Altaf, L. Huang, Y. Gao, Q. Wang, *J. CO2 Util.* **2020**, *35*, 90.

[46] H. S. Jeon, J. Timoshenko, C. Rettenmaier, A. Herzog, A. Yoon, S. W. Chee, S. Oener, U. Hejral, F. T. Haase, B. Roldan Cuenya, *J. Am. Chem. Soc.* **2021**, *19*, 7578.

[47] M. Li, M. N. Idros, Y. Wu, T. Burdyny, S. Garg, X. S. Zhao, G. Wang, T. E. Rufford, *J. Mater. Chem. A* **2021**, *35*, 19369.

2200046 (9 of 9)